ILASS 2008
Sep. 8-10, 2008, Como Lake, Italy

Paper ID ILASS08-2-11

MODELING DENSE SPRAYS USING BOUNDARY ELEMENT METHODS

Kisun Park[1], Stephen D. Heister[2]

School of Aeronautics and Astronautics, Purdue University
701 W. Stadium Ave., W. Lafayette, IN 47907-2045, USA

ABSTRACT

An axisymmetric boundary element method(BEM) has been developed to simulate atomization procedure in a pressure swirl atomizer. The formation of satellite drops was incorporated in the post-processing code via a nonlinear analysis of the ring-shaped ligaments formed in primary atomization events. The resultant tool provides a capability to generate spray distributions from first principles. The results show the resolution value ΔD typically used in experiments can not resolve dense satellite drops well in the distribution curve. The model for a pressure swirl atomizer including weak viscous treatment and satellite drops formation was validated against experimental results for air core radius, half cone angle, SMD, and drop size distribution. In addition, a quasi-3-D spray visualization is presented for a pressure swirl atomizer generating over 80000 drops .

1. INTRODUCTION

The atomization field has typically relied on empirically-based models for prediction of droplet sizes generated from a particular atomizer type. This process requires tedious measurements at a range of flow conditions and the resultant correlations are presumed to hold only for that particular injector/atomizer geometry that was tested. Moreover, historical modelling of the spray may simply use a representative (Sauter mean) diameter rather than a replication of the entire drop size distribution.

Higher level spray models have typically employed variety of distribution functions (Rosin Ramler, Nukiyama-Tanasawa, etc.) to provide an analytic description of the spray that requires only a few inputs from experimental measurements. Unfortunately, simulations of many engineering problems display a high degree of sensitivity to the overall distribution within the spray thereby placing substantial requirements on the modeller to improve the distribution functions to the greatest extent possible. For example, in combustion problems, the ignition kinetics are dominated by the smallest drops while the overall combustion time/efficiency is chiefly determined by the largest drops, i.e. the tails of the distribution function are terribly important to the overall modelling result.

For these reasons, there is a strong motivation to develop spray distributions from first principles such that the vagaries of the fitting of the distribution function are no longer an issue. The ever-increasing computational power now affords modelers a limited capability to conduct such simulations and that serves as the motivation for the subject work.

The classical swirl injector has been selected as an ideal testbed for the development of analytic/computational spray distributions because these injectors produce a reasonably axisymmetric swirling sheet that serves as the initial condition for atomization events. Presumably, there may be some success in making the assumption that portions of the atomization problem in this instance are axisymmetric, i.e. that ring-shaped ligaments are formed and those ligaments subsequently fractionate into drops. There is some experimental evidence to indicate that ligaments of this type are formed, although they generally do not extend around the full circumference of the sheet.

In the current work, a boundary element model (BEM) simulation of the atomization process is developed on this basis. The model is briefly described in the following section, followed by results, comparisons with measured data, and conclusions from the study.

2. MODEL DESCRIPTION

We provide only a brief description of the model in the interest of brevity. Interested readers are referred to References 1, 2, and 3 for a complete description of the model elements. An axisymmetric BEM formulation has been developed with arbitrary tracking of highly distorted free surfaces including a progression through individual atomization events. The surface is fit with cubic splines and curvature and nodal positions are determined with full 4^{th} order accuracy to provide a capability for high resolution. While the basic treatment is inviscid, weak viscous forces are included using the approach of Lundgren and Mansour[4].

The Laplace equation governs the inviscid base flow for the velocity potential and Green's functions resulting from the axisymmetric solution involve elliptic integrals that are curvefit as a function of their arguments to accuracy of 10^{-8}. Swirling flows are considered via a superposition of a potential vortex with the base flowfield. The Bernoulli equation

[1] Graduate Research Assistant, sunnypark@purdue.edu
[2] Professor, heister@ecn.purdue.edu

provides a boundary condition at the free surface and relates capillary, hydrostatic, centrifugal, and dynamic pressure forces to the local surface shape. The surface position is advanced in time via a set of kinematic relations for the local velocities.

Thin axisymmetric rings are shed from the parent sheet as a result of the primary atomization process. High surface curvature near regions of ring formation leads to substantial ring-to-ring variation thereby creating stochastic-type data from a deterministic computation. The rings are analyzed as rotating cylinders using a nonlinear BEM[3] and the resultant conlumn breaks into main and satellite droplets depending on its initial diameter and rotation rate. Assuming droplets are formed instantaneously as a result of this process permits subsequent quasi-3-D tracking of the spray.

3. RESULTS AND DISCUSSION

3.1 Grid system and geometry of a simplex nozzle

The pressure-swirl atomizer is often called 'simplex nozzle'. The simplex nozzle consists of three main parts; tangential inlet ports, swirl chamber, and exit orifice. An exit orifice is preceded by a swirl chamber with a certain contraction angle. Several inlet ports are attached to a swirl chamber tangentially, and the liquid flow is coming through these tangential inlet ports. The swirling flow within the swirl chamber causes a core of air to be formed at standard operating conditions and the air-core propagates to the outside of orifice such that a thin annular cone-shaped exit flow is created.

Figure 1 shows a schematic of a simplex nozzle with four tangential inlet ports. Here, r_s and l_s are the radius of swirl chamber from the axis of symmetry and the length of swirl chamber respectively. The variables, r_o and l_o, are the radius and the length of exit orifice respectively, which r_p and r_{pc} are the inlet radius of tangential port and the radial location of tangential port from the axis of symmetry respectively. Finally, θ_s is the contraction angle of swirl chamber and l_p is the length of tangential port.

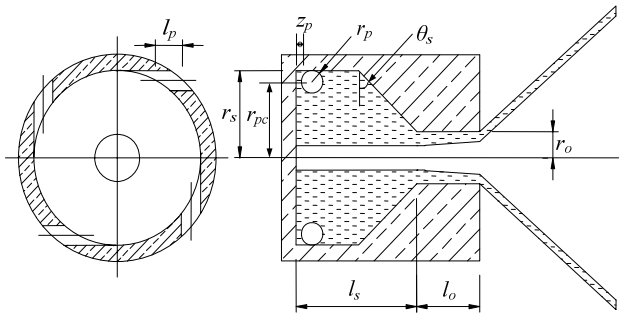

Figure 1. Schematic of a simplex nozzle with geometrical notations

All variables except the width of inlet port w_p should be given for the calculation. For 2-D axisymmetric calculation, an equivalent axisymmetric inlet slot is used assuming similar inlet areas. Some of experimental studies used inlet ports as many as possible in order to make flow coming through inlet ports to be very closely tangential to swirl chamber. Although a number of inlet ports may ensure the tangential velocity under experimental view point, inlet flow should be treated 3 dimensionally in computational view point for accurate calculation because the flow coming through a couple of inlet ports is not converted completely to circumferential flow. Therefore, the width of inlet slot, w_p, can be calculated as follows:

$$w_p = \frac{1}{2}\frac{n_p r_p^2}{r_s} \tag{1}$$

Unfortunately, most studies do not provide l_p and z_p. Thus, l_p and z_p are chosen within reasonable bounds under the revealed fact that the variation of inlet port do not significantly affect downstream flow conditions by parametric studies[5].

The initial grid system for a pressure swirl atomizer is illustrated in Figure 2. The initial grid system is constructed with given geometric parameters. It is noted that the grid system is changed due to the propagation of free surface to outside. The grid system is re-constructed at every time step via a cubic spline interpolation with a given grid spacing Δs. Therefore, the number of nodes on free surface increases as the conical sheet lengthens and decreases when a ligament is pinched off.

All geometrical parameters are nondimensionalized standard variables by the exit orifice radius r_o. A total of 105 fixed node points are used to describe the wall geometry. The contact point between the wall and the free surface inside the injector is required to be treated differently from other node points in order to simulate air-core inside injector. This corner is treated as a moving grid point. As this corner moves, the grid space along the wall is stretched in order to compensate the shifted distance. Therefore, gas core radius inside injector appears naturally.

A fictitious hemispherical cap is assumed for the end of the free surface. This cap is shed with the first ligament pinching-off event and after several pinching-off events memory of the initial condition is lost.

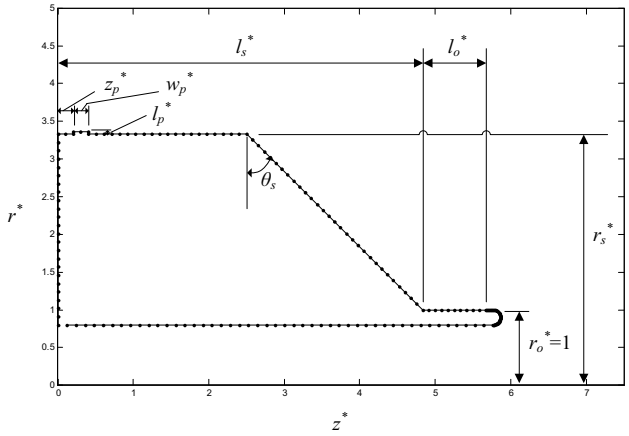

Figure 2. Schematic of the grid system for a simplex nozzle

3.2 Characteristic parameters for jet and droplets

Figures 3 illustrates the geometrical performance parameters for a simplex nozzle. Due to the swirl in swirl chamber produced from the flow coming through tangential inlet ports, the flow forms a thin film and therefore, forms an air core along the entire injector. The parameters, r_{a1}, r_{a2} and r_{a3}, represent air core radius in the swirl chamber, at the entrance of orifice, and at the exit of orifice respectively. The parameters, t_1 and t_2, represent film thickness at the entrance of orifice and at the exit respectively. The half cone angle θ is defined as the angle from the axis of symmetry to the first order polynomial fit to the upper surface here.

The SMD (Sauter Mean Diameter) is calculated for the statistical characteristic of a simplex nozzle. The SMD is calculated from original diameter of droplets which is generated after the flow is fully developed using the equation as follows:

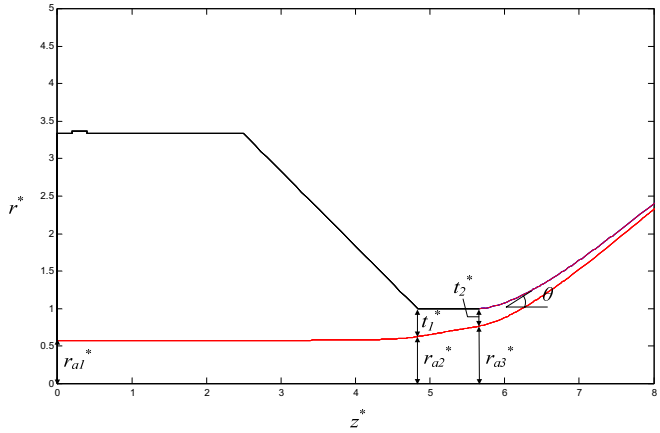

Figure 3. Critical characteristic parameters for a simplex nozzle

$$SMD = \frac{\Sigma ND^3}{\Sigma ND^2} \tag{2}$$

where N is the number of drops and D is the diameter of drops. Because the simulation gives the exact size of drops at each pinching event, the calculation like above equation is possible. Experimentally, drop size distributions are constructed by adding the number of drops within a given bin size, ΔD. Typically ΔD lies between 30-40 μm for generating distribution curves from experimentally[6]. In order to compare modeling results on this basis, a fitted SMD value is computed as follows:

$$SMD_f = \frac{\int_0^\infty D^3 (dN/dD) dD}{\int_0^\infty D^2 (dN/dD) dD} \tag{3}$$

where dN/dD is a fitted drop size distribution function to given drop size data.

3.3 Grid convergence study

H. Park[3] has substantially modified the previous BEM code for axisymmetric simulation of pressure swirl atomizer. Park was able to simulate the grid size ranges from 0.024 to 0.040 using SOR(Successive Over Relaxation) method. His results showed the reduction of SMD according to the grid size reduction, but it was not enough to confirm the grid convergence. To confirm the grid convergence on SMD, the simulation for 0.020 Δs and fewer Δs is required. By applying ScaLAPACK within the linear system solver, a significant reduction of simulation time is observed. This reduction of simulation time makes it possible to simulate the small grid size cases and achieve grid convergence on SMD.

The test condition for grid convergence test is given in Table 1. The grid size varies from 0.016 to 0.032 with increments of 0.004. The simulation time is from 0s to 10.1s. In the prior simulation[3], a large grid size(Δs = 0.032) is used from 0 s to the fully developed point, then a smaller grid size is used to obtain drop statistics. In this work, the code is run with a constant grid size from the start in order to reduce the possibility of perturbations in grid size affecting results.

Table 1. Geometry and flow conditions for grid convergence

Parameters	Dimensions	Parameters	Dimensions
r_s	2.0 mm	n_p	3
l_s	2.9 mm	w_p	0.12 mm
θ_s	45 deg	U_{in}	5.13 m/s
r_o	0.6 mm	We	447.9
l_o	0.5 mm	Re	1861.1
r_p	0.4 mm	Ro	1.0
l_p	0.018 mm	Bo	0
z_p	0.12 mm		

The detailed flow characteristics are shown in Table 2. There is no discernable difference in half cone angle, film thickness, air core radius. Obviously, these results show that internal free surface characteristics are not sensitive to grid size of range from 0.016 to 0.032.

Table 2. Characteristic parameters according to the grid size

Δs	0.032	0.028	0.024	0.020	0.016
Θ (deg)	37.8	38.3	38.3	38.2	38.3
t_1 (mm)	0.225	0.224	0.225	0.225	0.225
t_2 (mm)	0.138	0.138	0.138	0.138	0.138
r_{a1} (mm)	0.346	0.346	0.346	0.346	0.346
r_{a2} (mm)	0.375	0.376	0.375	0.375	0.375
r_{a3} (mm)	0.462	0.462	0.462	0.462	0.462
SMD (μm)	73.3	62.7	53.4	49.0	46.9
SMD_f (μm)	113.2	102.3	81.0	71.5	58.5
N_D	12294	17688	19215	29251	40596

In statistical properties, the most closely connected statistical property to the original results of code is SMD, which is calculated from drops generated after the flow is fully developed. The simulation gives the exact size of drops at its pinching event and then SMD is based on the diameters of each individual drop. It is found that the difference of SMD value becomes smaller with the decrease of the grid size. Therefore, it can be concluded that small grid size is required to get meaningful statistical properties.

SMD_f is calculated using trapezoidal integration on fitted curve to log-normal PDF. Unfortunately, the convergence of SMD_f is not confirmed. The reason is that small disturbance goes into results in the process of fitting. However, the grid convergence on SMD is already confirmed.

3.4 Code Validation – Flow characteristics

The simulation code for a simplex nozzle is validated here against experimental results provided by Halder *et al*[7]. For the simulation under their experimental conditions, l_p, z_p, and l_s are assumed. The assumption of l_s is based on H. Park[3]'s investigation of the effect of the length of swirl chamber on downstream flow. Park showed that the length of swirl chamber has very small effect on downstream flow and explained that sufficiently fully developed flow before the entrance of orifice makes the downstream flow insensitive to the length of swirl chamber. So, with the sufficient amount of assumed swirl chamber length, it will not affect the downstream flow significantly.

Two cases which have different inflow conditions under same geometry are simulated for the comparison against experimental results. The experimental conditions are provided in Table 3. Water is the working fluid.

The grid size used in this simulation is 0.032 for fast simulation and this value does not affect the flow characteristics. The results are obtained at t=5s, which is the time at the end of flow developing process.

Table 3. Geometry and flow conditions for the simulation of Halder et al's experiment

Injector No.	H_1	H_2
r_s (mm)	4.0	4.0
l_s (mm, l_s^*=10.0)	10.0	10.0
θ_s (deg)	20	20
r_o (mm)	1.0	1.0
l_o (mm)	4.0	4.0
r_p (mm)	1.26	1.26
l_p (mm, l_p^*=0.01)	0.01	0.01
z_p (mm, z_p^*=0.01)	0.01	0.01
n_p	4	4
w_p (mm)	0.794	0.794
U_{in} (m/s)	6.882	11.707
We	324.878	940.035
Re	3849.206	6547.617
Ro	1	1
Bo	0	0

There is no discernable difference between the experimental results for H_1 and H_2. Halder *et al*[7] explained the reason of this trend is the counterweighing effects by increasing swirling strength and subsequent decay due to increasing frictional effect in the nozzle. This trend of experimental results is also shown in simulation result.

The comparison between experimental results and simulation results is provided in Table 4. There is no difference between the simulation results for H_1 and H_2. This same trend of simulation results can be explained by the same reason as Halder *et al*[7]. An increased inflow velocity is counterbalanced by increased viscous effect inside the nozzle and then no discernable difference between H_1 and H_2 is observed. It is also observed that the difference between experimental results and simulation results is small, and the prediction of r_{a2} is better than r_{a1}. It should be noted here that Halder *et al*[7] also showed that the air core radius increases with an increase of Reynolds number in low-Reynolds number region. For the complete code validation, it is required to simulate a case in a low-Reynolds number region. However, in a low-Reynolds number region, the numerical error should be considered significantly because the truncation error of weak viscous treatment is proportional to $Re^{-3/2}$.

Table 4. Comparison of experimental results and simulation results for the simulation of Halder et al's experiment

	H_1		H_2	
	Exp.	Sim.	Exp.	Sim.
r_{a1} (mm)	0.331±3.28%	0.271	0.575±3.28%	0.556
r_{a3} (mm)	0.331±3.28%	0.271	0.575±3.28%	0.556

Without consideration of viscous effect, H. Park[5] already showed the increase of film thickness according to increasing ΔP across the nozzle as it is described in Figure 4. Therefore, it can be concluded that weak viscosity treatment works well in a higher Reynolds number region.

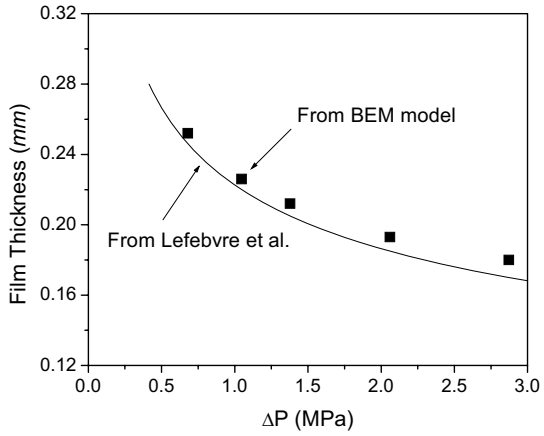

Figure 4. Variation of film thickness with injectior pressure, comparison between a experimental results[9] and model calculation without viscous effects[5]

3.5 Code validation - Statistical properties

The simulation code for a simplex nozzle is validated here against experimental results provided by Cousin *et al*[8]. Their experimental conditions are provided in Table 5. The experiment is performed on four injectors which have different orifice radius with ΔP = 10 bar for cone angle, SMD, and drop size distribution. The fluid used in experiment is water.

Due to computational constraint, Δs=0.024 is used for injector J_1, Δs=0.020 is used for injector J_2, and Δs=0.016 is used for injector J_3 and J_4. Using Δs=0.016 may be the best choice for getting converged SMD, but large computational time is required for this small Δs. For the simulation of injector J_1, it takes approximately 30.3 days to obtain a result up to t = 8 s. In case of J_2, 46.2 days are spent for the simulation up to t = 8 s. 45 days are spent for the simulation of J_3 up to t = 8 s and 15.8 days are spent for the simulation of J_4 up to t = 10 s.

Table 5. Geometry and inflow conditions for the simulation of Cousin *et al*'s experiment

Injector No.	J_1	J_2	J_3	J_4
r_s (mm)	3.5	3.5	3.5	3.5
l_s (mm)	5	5	5	5
θ_s (deg)	90	90	90	90
r_o (mm)	0.5	0.6	0.75	1.0
l_o (mm)	1	1	1	1
r_p (mm)	0.5	0.5	0.5	0.5
l_p (mm) (l_p^*=0.03)	0.015	0.018	0.0225	0.03
z_p (mm) (z_p^*=0.2)	0.1	0.12	0.15	0.2
n_p	6	6	6	6
w_p (mm)	0.214	0.214	0.214	0.214
U_{in} (m/s)	3.578	4.508	5.534	7.752
We	87.806	167.259	315.073	824.328
Re	2001.118	3025.503	4642.617	8671.140
Ro	1	1	1	1
Bo	0	0	0	0

The results of simulation and experimental results on half cone angle and SMD are compared in Table 6. The half cone angles calculated using BEM code show a good agreement with experimental results for all injectors. The SMD from simulations is pretty smaller than the result of experiment for all injectors. Approximately, the difference is from 20 μm to 30 μm. This difference mainly comes from satellite drops. As it can be observed in drop size distribution plot, Figure 5, the drop size distribution of simulation is shifted slightly to the left of experimental results and overall shape of it is narrower than experimental results. As explained in section 3.6, due to the limitation of measuring device, satellite drops may be significantly underestimated in experimental results. In addition, the concentrated region in a small drop size range can not be detected due to the limited detectable drop size range ΔD. Therefore, due to the presence of large amount of satellite drops in simulation results, the distribution is shifted to the left and the calculated SMD is smaller than measured value.

Table 6. Comparison of experimental results and simulation results for the simulation of Cousin et al's experiment

	Experiment		Simulation	
	θ (deg)	SMD (μm)	θ (deg)	SMD_f(μm)
J_1	30	102	29.5	84.4
J_2	29	118	32.3	84.0
J_3	34	114	35.4	85.5
J_4	36	135	39.3	112.4

One thing should be noted here is that Δs used in J_1 and J_2 is 0.024 and 0.020 respectively. As it is shown in grid convergence section, SMD is much related to the grid size. When large Δs is used in simulation, corresponding SMD is bigger than the converged SMD with small Δs. Therefore, SMD corresponding to 0.024 and 0.020 is bigger than SMD corresponding to 0.016. This is the reason why SMD on J_1, J_2, and J_3 are all similar to each other. So, it can be expected that SMD on J_1 and J_2 will be smaller than current value and the tendency of SMD change between injectors follows the tendency of SMD change in experimental results if 0.016 is used for Δs in J_1 and J_2.

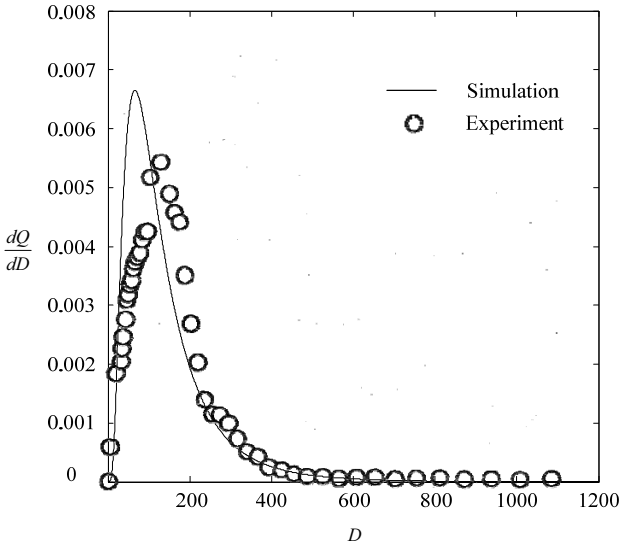

Figure 5. Comparison of volumetric distribution between experimental result and simulation result for J_1

3.6 Bimodality of drop size distribution

The formulation of satellite droplets from a rotating column is used to study the effect of satellite drops in the present model.

The drop size distribution under the same simplex nozzle as the nozzle of grid convergence study is illustrated in Figure 6. Figure 6 is number PDF histogram for satellite drops and main drops collected after the flow field is fully developed. Because a fictitious hemispherical cap at the end of the conical sheet is utilized for the initial shape of free surface, drops collected in transient region are not used for drop size distribution. The grid size Δs used in this simulation is 0.016, and this means that SMD for drops collected after the flow is fully developed converged with grid size as it is explained in the following grid convergence section.

The drop size distribution is obtained by histogram whose individual bin is representing the number of drops within the width of drop size range ΔD. Experimentally, ΔD is determined by measuring equipment and the accuracy of PDF plots is highly related to this quantity. While in principle the BEM result gives the exact size of drops at every pinch-off event, comparison against experimental data necessitates the use of similar bin sizes (ΔD value). We desire small ΔD in the drop size histogram so that the good accuracy is possible in the plot. Until now, most studies have shown that the drop size distribution often follows unimodal distribution such as log-normal or log-hyperbolic, etc. The present calculations show interesting changes in distributions depending on the ΔD value employed. For example, Cousin et al[8] have generated their volume PDF plot whose the range is a factor of 40 μm using laser diffraction based Malvern 2600 D particle sizer.

It is difficult to identify which distribution curve it follows due to the irregularity of the height of bins in Figure 6. When large ΔD is used, i.e. 12.5 μm, a nearly unimodal distribution is obtained. The fitted log-normal curve to the histogram whose ΔD is 12.5 μm is presented in Figure 7. However, results show a closeness to bimodal distribution in the case of small ΔD. The first peak point is located at around 10 μm. This peak is contributed by satellite drops formulation. The second peak point contributed by main drops is located at around 30 μm. Because there is no theoretical basis for measuring bimodality, it is difficult to determine which distribution curve shows a good agreement with the given data set. So, the way to compare errors produced after the data is fitted to bimodal distribution curve and log-normal distribution curve is used for checking bimodality. The bimodal distribution function is given as follows:

$$f(D)=\frac{P}{\sqrt{2\pi}s_{n,1}}e^{-\frac{1}{2}\left(\frac{D-\overline{D}_1}{s_{n,1}}\right)^2}+\frac{1-P}{\sqrt{2\pi}s_{n,2}}e^{-\frac{1}{2}\left(\frac{D-\overline{D}_2}{s_{n,2}}\right)^2} \quad (4)$$

This bimodal distribution function represents the mixture of two different normal distributions. The variables, $s_{n,1}$ and $\overline{D}_1$, represent a deviation and mean value for first normal distribution respectively and $s_{n,2}$ and $\overline{D}_2$ are for second normal distribution. The variable P is the value for the normalization. The error for the fitted curve is defined as follows:

$$E=\left(\sum (Y_i-y_i)^2\right)^{\frac{1}{2}} \quad (5)$$

where Y_i is the actual data and y_i is the data on the fitted curve.

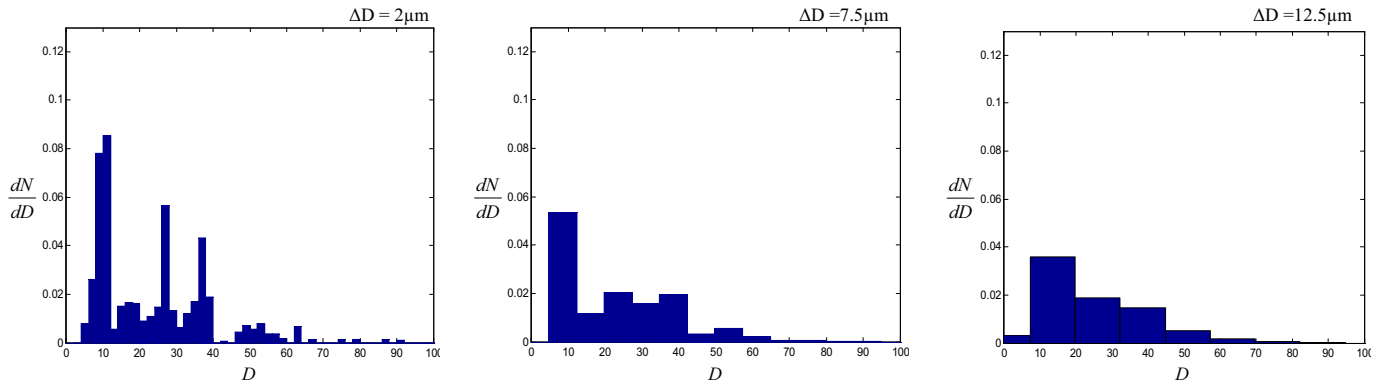

Figure 6. Number PDF distribution of main and satellite drops for the nozzle used in grid convergence study with variation of ΔD

The function *fminsearch* in MATLAB is used to find the minimum error bimodal distribution function of five variables which is corresponding to the original given data set. The help of MATLAB said that the function *fminsearch* is generally referred as 'unconstrained nonlinear optimization'. Only ΔD=2 μm case including main and satellite drops was able to be insensitive to initial guess. Because the unconstrained nonlinear optimization method can have several local optimums, it is pretty important to check that the converged solution by *fminsearch* is consistent with a desired shape of function.

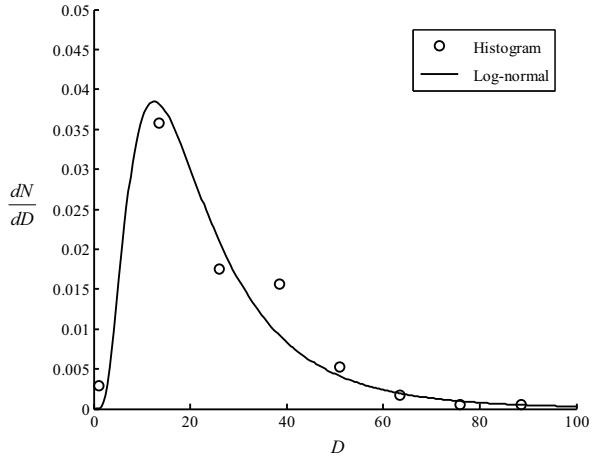

Figure 7. Comparison of fitted log-normal curve and histogram of 12.5 μm ΔD for main and satellite drops

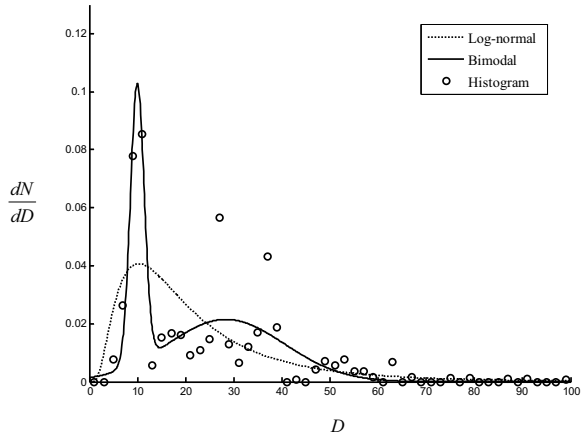

Figure 8. Number PDF distribution of main and satellite drops for ΔD=2 μm fitted to bimodal and log-normal distribution

Figure 8 shows log-normal distribution and bimodal distribution fitted to ΔD=2 μm case including main and satellite drops. The peak point values are pretty much different from each other. The first peak point value in histogram is around 0.08 at 10 μm. This point appears in bimodal distribution fitting and the value is slightly bigger than the value from the histogram. In case of log-normal fitting, it shrinks to small value to be balanced with other small values which are placed by peak value. The second peak point value which is placed at around 30 μm in histogram is much underestimated in log-normal fitting.

The error for bimodal distribution is 0.05143 and the error for log-normal distribution is 0.09691. Therefore, it can be concluded that the original data set for this case is slightly closer to bimodal distribution than unimodal distribution. This is one of interesting aspects of pressure swirl atomizer which are revealed by the simulation using BEM code. As explained above, most studies indicated that sprays from pressure swirl atomizer follow unimodal distribution. One of reasons for this, their measuring device is not good for measuring dense sprays. PDPA(Phase/Doppler particle analyzer) and diffraction based measurement are commonly used for measuring the size of drops formed from pressure swirl atomizers. Blaisot and Yon[10] indicated that these measurement are difficult to measure dense sprays, i.e. diesel sprays, due to multi-scattering effects, high drop velocity and concentration and nonspherical shapes. The other reason is that the limitation of detectable drop size range results in underestimation of small satellite drops. For example, Cousin *et al*[8]'s measuring device has detectable drop size ranges from 11.6 μm to 1128 μm. This feature can cause significant underestimation of drops under 11.6 μm. In addition, due to the limitation of size range ΔD of measuring device, the concentration of drops in a small range is not detectable. This causes a significant underestimation at a peak point so that the peak does not show up in distribution plot.

3.7 3D jet and droplets visualization

On the basis of droplet tracking scheme developed by H. Park[5], quasi-3-D visualization of jet is possible. Newton's 2nd law is applied in the tracking scheme to describe the motion of a droplet against aerodynamic drag force. The governing equation for the motion of a droplet is as follows:

$$m_D \frac{d\vec{u}_D}{dt} = C_D \frac{1}{2} \rho_g \left|\vec{u}_D\right|^2 A_D \qquad (6)$$

where A_D is the projected area of a droplet($\pi D^2/4$), m_D and $\vec{u}_D$ is droplet mass and velocity, respectively. The drag coefficient C_D is given by Hwang et al[11]:

$$C_D = \begin{cases} \frac{24}{\mathrm{Re}_D}(1+\frac{1}{6}\mathrm{Re}_D^{1/3}) & \mathrm{Re}_D \le 1000 \\ 0.424 & \mathrm{Re}_D > 1000 \end{cases} \quad (7)$$

where $\mathrm{Re}_D = U_R D \rho_{air} / \mu_{air}$ where U_R is a relative velocity between droplet and air.

The second order ordinary differential equation (6) is transformed to a system of first order ODEs, and then 4th order Runge-Kutta time marching scheme is utilized to solve first order ODEs. Collision between droplets, vaporization, and the velocity of air (momentum interchange between fluids) are neglected here. After the droplet tracking is done three dimensionally, the shape of jet and droplets is visualized by Tecplot. While droplets being visualized by Tecplot, each droplet represents one zone so that the same number of zones is required as the number of droplets to be visualized. Unfortunately, the number of zones which can be presented at one time is limited to 32700 by Tecplot. Therefore, droplets are divided into several sets containing the drops less than 32700 and then each set is drawn in a picture file and the sets for the drops generated at the same simulation time are integrated into a picture file by Photoshop. Due to the limitation of available number of zones in Tecplot, the formation of satellite drops is not considered in the visualization.

The shape of the flow field of Cousin *et al*'s injector J_4 at t=10s is presented in Figure 9. At this time, total number of droplets contained in the picture is about 82000.

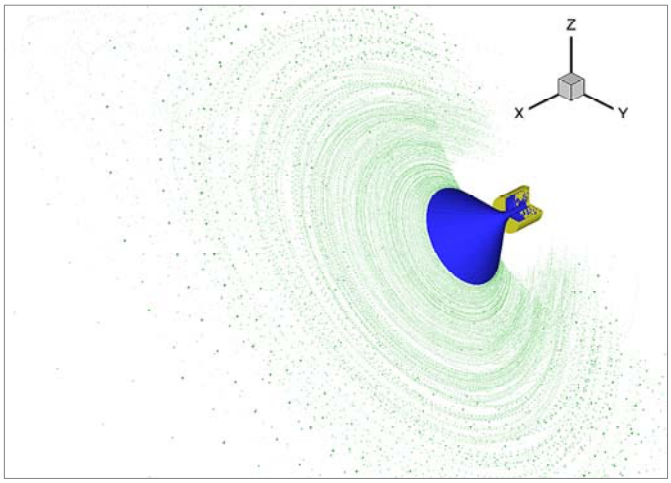

Figure 9. Spray simulation for Cousin *et al*'s injector J_4 at t=10s, total N_D is about 82000

4. CONCLUSIONS

An axisymmetric boundary element method, in concert with a nonlinear secondary atomization simulation of ring-shaped ligaments has been developed to provide first-principles spray simulations of the pressure swirl atomizer. Grid convergence has been demonstrated on the basis of SMD for typical injector performance range. The model for a pressure swirl atomizer including weak viscous treatment and satellite drops formation was validated against experimental results for air core radius, half cone angle, SMD, and drop size distribution. The simulation results showed good agreement with experimental results.

The formation of satellite drops was incorporated in the post-processing code to investigate the effect of satellite drops on the drop size distribution curve. An interesting result was observed, which is that the drop size distribution curve from BEM code for a pressure swirl atomizer is closer to bimodal distribution rather than unimodal distribution with a small width of droplet diameter range ΔD. It was also found that the drop size distribution curve follows a unimodal distribution with a large ΔD such a value used in the experiment. Thus, it was found that resolution values typically used in experiments cannot resolve satellite drops. Finally, using prior droplet tracking algorithms[5], three dimensional spray visualization was done for a pressure swirl atomizer generating over 80000 drops with the help of ScaLAPACK.

NOMENCLATURE

n_p	number of inlet ports
U_{in}	inflow velocity (m/s)
We	Weber number
Re	Reynolds number
Ro	Rossby number
Bo	Bond number
N_D	number of droplets
Δs	grid spacing
ΔD	drop size range
SMD	Sauter Mean Diameter
S_n	geometric standard deviation
$\bar{D}$	geometric number mean drop size

Superscripts

$( )^*$	nondimensional parameter

REFERENCES

[1] J. H. Hilbing, S. D. Heister, and C. A. Spangler, A Boundary Element Method for Atomization of a Finite Liquid Jet, *Atomization and Sprays*, Vol. 5, 6:621-638, 1995.

[2] S. S. Yoon and S. D. Heister, A Fully Nonlinear Model for Atomization of High-Speed Jets, *Engineering Analysis with Boundary Elements*, 28:345-357, 2004.

[3] H. Park and S. D. Heister, Nonlinear Simulation of Free Surfaces and Atomization in Pressure Swirl Atomizers, *Physics of Fluids*, Vol. 18, 052103, 2006.

[4] T. S. Lundgren and N. N. Mansour, Oscillations of Drops in Zero Gravity with Weak Viscous Effects, *Journal of Fluid Mechanics*, 194: 479-510, 1988.

[5] H. Park, *Flow Characteristics of Viscous High-Speed Jets in Axial/Swirl Injectors*, PhD thesis, Purdue University, 2005.

[6] A. H. Lefebvre, Atomization and Sprays, *Taylo & Francis*, 1989.

[7] M. R. Halder, S. K. Dash, and S. K. Som, Influences of Nozzle Flow and Nozzle Geometry on the Shape and Size of an Air Core in a Hollow Cone Swirl Nozzle, *Journal of Mechanical Engineering Science*, Vol. 217, Part C, 2003.

[8] J. Cousin, S. J. Yoon, and C. Dumouchel, Coupling of Classical Linear Theory and Maximum Entropy Formalism for Prediction of Drop Size Distribution in Sprays: Application to Pressure-swirl Atomizers, *Atomization and Sprays*, 6:601-622, 1996.

[9] N. K. Rizk and A. H. Lefebvre, Internal Flow Characteristics of Simplex Swirl Atomizer, Journal of Propulsion and Power, Vol. 1, No. 3, pp.193-199, 1985.

[10] J. B. Blaisot and J. Yon, Droplet Size and Morphology Characterization for Dense Sprays by Image Processing: Application to the Diesel Spray, *Experiments in Fluids*, 39:977-994, 2005.

[11] S. Hwang, Z. Liu, and R. D. Reitz, Breakup Mechanisms and Drag Coefficients of High Speed Vaporizing Liquid Drops, *Atomization and Sprays*, 6:353-376, 1996